A Spectrographic Search for Colliding Stellar Winds in O-Type Close Binary Systems. V. HD 149404 ~

M. L. Thaller[1]
Infrared Processing and Analysis Center
California Institute of Technology
Pasadena, CA 91125;
thaller@ipac.caltech.edu

D. R. Gies
Center for High Angular Resolution Astronomy
Department of Physics and Astronomy
Georgia State University
Atlanta, GA 30303;
gies@chara.gsu.edu

A. W. Fullerton[2]
Department of Physics and Astronomy
University of Victoria
Victoria, BC V8W 3P6, Canada;
awf@pha.jhu.edu

L. Kaper
Astronomical Institute "Anton Pannekoek"
University of Amsterdam
Kruislaan 403
1098 SJ Amsterdam, The Netherlands;
lexk@astro.uva.nl

R. Wiemker
Philips Forschung Hamburg
Medical Image Analysis
Roentgenstrasse 24-26
D-22335 Hamburg, Germany
R.Wiemker@pfh.research.philips.com

---

[1]Visiting Astronomer, Mount Stromlo and Siding Springs Observatories, Australian National University

[2]Postal Address: FUSE Science Center, Department of Physics and Astronomy, The Johns Hopkins University, 3400 N. Charles St., Baltimore, MD 21218

Michelle, Sorry the toner cartridge was low!
What do you think? Cheers, Doug

ABSTRACT

We present new Hα emission line spectra and an analysis of the mass outflow for the massive close binary, HD 149404. Spectra obtained between 1995 and 1997 show evidence of coherent orbital phase-related variations superimposed upon both long term and short term emission strength variations. We use a Doppler tomography algorithm to construct velocity maps of the emission intensity, and these demonstrate that emission displays two broad peaks that follow sinusoidal radial velocity curves that are significantly different from the orbital velocity curves of either star. We present a model for the kinematics and distribution of the emitting circumstellar gas, and we argue that most of the emission comes from wind flows from both stars into a shock region region between them. The binary appears to be in a post-mass transfer stage in which systemic mass loss dominates evolutionary processes.

Subject headings: line: profiles – stars: binaries: close — stars: binaries: spectroscopic — stars: early-type — stars: individual (HD 149404) — stars: mass-loss

1. Introduction

Radiatively driven winds are found in all massive luminous stars, and in close binary systems, the individual winds may collide and form a bow shock which wraps around the star with the weaker wind. One easily observable consequence of colliding winds is Hα emission. This emission is an excellent probe of dense regions in the wind, as it is caused by recombination, in which the emissivity scales with the square of the density. Enhanced density is expected in two places, the lower layers of the wind near the photosphere of the generating star, and near the shock. The lower wind contribution to Hα comes from layers typically between 1.0 and 1.5 stellar radii (Puls et al. 1996). Such base level emission will show radial velocity variations similar to the stars themselves. Emission formed in the shock region, on the other hand, will display velocity variations defined by the spatial and velocity structure of the circumstellar gas. These velocity curves are often quite different from the motion of the stars. Several groups have made Hα studies of massive binary systems and deduced the presence of colliding winds (Vreux 1985; Gies & Wiggs 1991; Wiggs & Gies 1992, 1993; Gies, Wiggs, & Bagnuolo 1993).

Thaller (1997) undertook an all-sky Hα survey of massive binaries to search for likely colliding winds candidate systems. She identified HD 149404, a system containing two massive evolved stars locked in a close orbit, as an especially promising system for the detection of wind-induced shocks. HD 149404, composed of a supergiant and giant star, is one of the brightest members of the Ara OB1 association. Hα emission was first observed by Kucewicz (1963), and a double-peaked structure to the emission was observed by Jaschek, Jaschek, & Kucewicz (1964), suggesting that HD 149404 was a binary. Supporting this notion, Hutchings (1976) found HD 149404 to be a radial velocity variable. Conti, Leep, & Lorre (1977) discovered a double-lined spectrum for the system, and the first orbital elements were determined by Massey & Conti (1979), who set the period at 9.813 days. Massey & Conti hypothesized that the Hα emission seen in this system could be indicative of current large mass loss. They determined that the brighter star (estimated to be an O8.5 I) was less massive than the dimmer, hotter star (O7 III(f)), which also suggested a history of mass-loss or mass-transfer. Stickland & Koch (1996) used cross-correlation techniques with UV spectra from the *International Ultraviolet Explorer* satellite and found a similar period of 9.8145 days, again with the dimmer star as the more massive component ($M_2/M_1 = 1.53 \pm 0.09$). In addition, Stickland & Koch (1996) noticed a strengthening of the lines of the dimmer star during its quadrature of greatest blue-shift, a classic "Struve - Sahade Effect" (Gies et al. 1997). HD 149404 is also a known *IRAS* infrared source and a radio emitter at 3.6 cm (Lamers & Leitherer 1993). further indications of extensive mass loss and the likely presence of circumstellar material in the system. This system presents an interesting problem to stellar nomenclature. The brighter star was originally identified as the "primary" star. while in fact, the dimmer star is the more massive (and hotter) of the two. In order to avoid confusion in this paper, the bright supergiant star will be referred to as "Star 1" and the dimmer, more massive giant star, "Star 2." Note that the system has no known close visual companion (Mason et al. 1998), so that we can assume that the spectral features form only in these two stars and their immediate vicinity.

The basic properties of HD 149404, as well as its exact evolutionary status, are subject to considerable debate. Using a tomography technique to separate the individual spectra (Bagnuolo, Gies, & Wiggs 1992), Penny (1996) obtained spectral types of O8.5 I and O6.5 III using UV classification criteria. Penny then used the single star evolutionary tracks of Schaller et al. (1992) to estimate the masses of the stars, $M_1 = 44 \pm 5$ and $M_2 = 49 \pm 12$ $M_\odot$, and their ages, ≈ 3 million years. Using her estimate of the inclination ($i = 21°$), Penny determined that both stars in HD 149404 were rapid rotators, with nearly twice the synchronous rotation rate. While the advanced evolutionary state and low mass of Star 1 suggests mass-transfer has occurred in the past, the huge rotational velocities seem inconsistent with the dynamics of Roche Lobe overflow, which should force synchronous

rotation.

Hoping to resolve some of these inconsistencies, Penny, Gies, & Bagnuolo (1999) analyzed a light curve of HD 149404 from the *Hipparcos* satellite (ESA 1997). Although the variations in intensity are small (approximately 0.04), the light curve shows a clear ellipsoidal variation. No eclipses were observed, however, which placed a tighter constraint on the inclination of the system. Penny's new estimate ($i = 30°$) brought the stars' equatorial velocities down ($V_{eq\ 1} = 172$ and $V_{eq\ 2} = 109$ km s^{-1}), but still showed them to be rotating faster than synchronous. A major change, however, occurred in Penny's estimate of the stellar masses. With the new inclination, she estimated the masses to be 16 $M_\odot$ and 18 $M_\odot$ for Star 1 and 2, respectively. In addition, the new parameters suggest Star 1 is very close to filling its Roche lobe.

Penny et al. (1999) proposed that HD 149404 has experienced mass loss (or possibly mass transfer) in the past, which has now ceased. They suggest that Star 1, originally the more massive, lost mass through Roche lobe overflow, which may or may not have accreted onto the other star. This mass loss increased the mass ratio above unity, making Star 2 more massive, and led to greater separation of the stars. The current super-synchronous rotation rates may reflect the synchronous rotation of an earlier, shorter period system. The rotational velocities may partially account for the surprisingly low masses of the stars, as rapidly rotating stars have larger mass-loss rates than found in non-rotating stars (Maeder 1999). Penny's scenario agrees well with suggestions by Vanbeveren & de Loore (1980) and Hutchings & Van Heteren (1981) that Star 1 is a post-Roche lobe overflow object. The apparent lack of C III and extreme strength of the N III lines found by Jaschek & Jaschek (1974) also suggests past mass loss by Star 1, which has resulted in the exposure of nuclear processed materials at the surface of the star. In the UV region of the spectrum, however, Penny (1996) found normal carbon line strengths for the supergiant star, so the situation may not be that simple.

In this paper, we report on a detailed study of the orbital phase-related variations of the Hα line. We show that coherent emission variations are present, but have radial velocity patterns that differ from the orbital motion of either star. We present an analysis of these motions, aimed at determining the location of the emitting gas in the system.

2. Observations and Reductions

Two independent groups, one at Georgia State University (GSU) and one at the European Southern Observatory (ESO), obtained Hα spectra of HD 149404. The GSU

observations were obtained by M. Thaller with the 74-inch Telescope at Mount Stromlo Observatory on the nights of 1996 March 3–12, using the coudé spectrograph, grating C (600 grooves mm^{-1}, blazed at 12500 Å) in second order, and the 81.3 cm focal length camera. This produced a spectral coverage of 6648 – 6740 Å with a reciprocal dispersion of 0.24 Å $pixel^{-1}$ on a thinned 2048 × 2048 Tektronix CCD detector (Tek 2K). An RG610 filter was used to block higher orders. The exposure times ranged from 5 to 20 minutes depending on sky conditions, and several bias, flat field, and Th-Ar comparison lamp spectra were obtained each the night. In addition, several spectra of the rapidly rotating star HD 87901 were taken each night to facilitate later telluric division. A second run on the Mount Stromlo 74-inch Telescope took place on the nights of 1997 March 20 – April 1. The arrangement was identical to the first Mount Stromlo run, with the exception of the detector which was a 4096 × 2048 SITe CCD. This produced a wavelength coverage of 6342 – 6962 Å and a reciprocal dispersion of 0.152 Å $pixel^{-1}$. For both observing runs, we were able to obtain data with a signal-to-noise ratio of 200–300 $pixel^{-1}$ in the continuum.

L. Kaper, in collaboration with A. Fullerton, obtained Hα spectra for a large number of O-type stars, including HD 149404, at ESO with the Coudé Auxiliary Telescope and Coudé Echelle Spectrometer on the nights of 1995 May 29 – June 6, using the red-optimized path with CCD#31 (2048 × 2048 pixels), windowed to 40 pixels in the cross-dispersion direction, as a detector. This arrangement produced a spectral coverage of 6533 – 6594 Å with a reciprocal dispersion of 0.029 Å $pixel^{-1}$ and a typical signal-to-noise ratio of 250 $pixel^{-1}$. The spectra were wavelength calibrated using Th-Ar spectra obtained every 2 hours. These spectra were extracted, calibrated, and telluric-cleaned using the MIDAS software package.

The MSO data were extracted and calibrated using standard routines in IRAF[3]. Subsequently, the spectra were rectified to a unit continuum using a cubic spline fit to line-free regions. The spectra were then cross-correlated with a library of purely telluric spectra obtained from images of the rapidly rotating standard star. Each target spectrum was divided by the best-fit telluric spectrum, leaving the resulting spectrum free of atmospheric lines. Next, the spectra were cleaned of remaining cosmetic imperfections by interpolation. Finally, spectra from each run were interpolated onto a common heliocentric wavelength grid.

---

[3]IRAF is distributed by the National Optical Astronomy Observatories, which is operated by the Association of Universities for Research in Astronomy, Inc., under cooperative agreement with the National Science Foundation.

3. Variations in Hα Emission

We begin by considering the orbital phase-related variations in the spectra. We calculated orbital phases using the ephemeris of Stickland & Koch (1996): $P = 9.81452$ d and $T_0 =$ HJD 2,444,449.303 where zero phase corresponds to Star 1's maximum radial velocity in this circular orbit. A journal of observational dates and phases is given in Table 1. Figure 1 shows the ESO Hα spectra plotted as a function of orbital phase and radial velocity, assuming a rest wavelength of 6562.682 Å, while Figure 2 shows the same for the two MSO runs. The spectra are placed in the diagram so that their continua are aligned with the orbital phase of observation. The bar at the upper right indicates the intensity scale relative to the continuum. The Hα line shape shows a clear progression with orbital phase, changing from single- to double-peaked twice during the orbit. However, the patterns are not those expected from the orbital motion of the stars (see below).

Inspection of Figures 1 and 2 shows that there are also significant variations in Hα strength that are unrelated to orbital phase. The profile apparently changed in overall strength between 1995 and 1996-7. Equivalent widths (from numerical integration and with errors of $\approx 10\%$) are listed in Table 1 and plotted versus orbital phase in Figure 3. The emission strength appears to have increased from $W_\lambda = -4.6$ Å in 1995 to $W_\lambda = -6.5$ Å in 1996 and 1997. We doubt this has an instrumental origin (for example, from differences in scattered light) because observations of other binaries from ESO and MSO do not show this discrepancy. However, changes of this magnitude are seen in the Hα emission of some single O-supergiants (Kaper et al. 1998). The detailed profile shape also shows evidence of long-term changes (see, for example, the extended blue wing found in the MSO 1996 spectra in the phase range $0.0 - 0.3$). Furthermore, there are variations on time scales of days superimposed upon the orbital phase-related variations (see the large differences near line center at phase 0.4 between spectra obtained within the 1996 and 1997 runs). Thus, although we will focus attention on the orbital shape variations in the discussion below, the variations in equivalent width on other time scales clearly indicate that the outflows that produce the Hα emission are transitory in nature. Given these substantial variations, there is no compelling evidence that the emission equivalent width is phase dependent.

The lack of substantial equivalent width variations related to the orbital cycle suggests that no significant occultation of the emitting regions by the stars occurs during the orbit. This is not surprising given the system's low orbital inclination ($i = 30° \pm 5°$; Penny et al. 1999). The orbital phase variations in the shape of Hα appear to result from the changing viewing angle with orbital phase of a mainly optically thin emitting gas that has an anisotropic velocity distribution. Because the orbit is essentially circular (Stickland & Koch 1996), we expect than each element of gas in the volume will appear to show

orbital phase-related Doppler shifts dependent upon the motion of that element. It is also reasonable to assume that gas motions are symmetric with respect to the orbital plane.

These conditions are ideal for the application of a Doppler tomography algorithm to reconstruct the velocity distribution of the emitting gas using the ensemble of emission line profiles from around the orbit. Doppler tomography is now an important tool in emission line studies of cataclysmic variables (Kaitchuck et al. 1994) and Algol binaries (Richards, Jones, & Swain 1996), and it has a direct application in the current study. The algorithm seeks to find an emission intensity distribution in a velocity grid plane, (V_X, V_Y) (where X is defined by the axis joining the stars), such that the integrated emission as seen from various view angles (or back projections) matches the observed, one-dimensional emission profile. There are many approaches in medical imaging to solving this problem, and astronomers have generally embraced Fourier techniques that work well if the observations have good phase coverage (Kaitchuck et al. 1994). Our data sets have, unfortunately, some significant phase gaps, and so we have used instead an iterative least-squares technique that starts with an empty field and slowly builds up the emission distribution through corrections derived from the ensemble of observed emission profiles. This approach is a direct extension to an $N \times N$ reconstruction of the methods we have applied to the $N \times 2$ reconstructions used to separate the spectra of binary stars (Bagnuolo et al. 1992). The code was written in IDL[4] by E. Wiemker.

We chose to apply the tomography algorithm separately to the ESO and MSO data sets because of the overall change in emission strength observed between these epochs of observation. The first task in this application is to reset the continuum to a zero value, and then create a velocity grid corresponding to the "center of motion" of the emission. Ideally, this adopted central velocity would be equal to the systemic velocity of the binary. However, there is considerable uncertainty about the actual systemic velocity of HD 149404 because the spectral features measured for radial velocity participate in the photospheric expansion and wind outflow, and the resulting values cover the range from $V_0 = -28$ km s^{-1} to -60 km s^{-1} (Massey & Conti 1979; Stickland & Koch 1996; Penny 1996). We decided to find the central velocity from the profiles themselves by forming a global average of all the profiles from a run and then calculating the first moment of the average (equal to -40.3 km s^{-1} for the ESO set and -47.5 km s^{-1} for the MSO sets). We then ran the tomography algorithm for a projected velocity grid from -800 to $+800$ km s^{-1}: this amounted to a 233×233 (141×141) velocity grid image for the ESO (MSO) data. We took the viewing angles directly from the orbital phases listed in Table 1, and we ran the tomography

[4]IDL is a registered trademark of Research Systems, Inc.

procedure for 100 iterations with a gain of 0.8 (the results are insensitive to the values of either parameter).

The resulting tomograms are illustrated as grayscale images in Figures 4 and 5 for the ESO and MSO data sets, respectively. The grayscale intensity is shown as a fraction of the peak intensity in the tomogram (with identifying contour levels given), and for the purposes of illustration the image was rescaled omitting the lower 20% of emission intensity (which is partially marred by low level artifacts of the reconstruction). The observed emission profile at any given orbital phase is given by a projection through the image at a particular angle. For example, the projection for phase 0.25 corresponds to the projection from the top of the figure to the bottom. The tomogram predicts we observe at that phase a broad, double-peaked feature that is more intense at positive velocities, just as observed at this phase (Fig. 1). In fact, we made projections through the tomograms at the observed phases in order to directly compare the expectations from the reconstruction with the actual observations. These model back-projected profiles are shown as dashed lines in Figures 1 and 2, and they generally make a satisfactory match of the observations. This happy result gives us confidence that the tomograms are indeed an adequate representation of the Hα emission velocity distributions in HD 149404.

Figures 4 and 5 also show white circles which indicate the projected rotational velocity limits of the two stars in this velocity grid. We see that the emission has a fundamentally different velocity distribution from that of the two stars and, in fact, shows motions orthogonal to those of the stars. The emission distribution is centered more or less on the center of mass of the system, and both data sets shows subsidiary peaks which are distributed along the V_Y axis. There are two peaks in the ESO tomogram, a strong one centered near $V_X = -96$ km s^{-1} and $V_Y = -18$ km s^{-1} and a weaker peak near $V_X = +116$ km s^{-1} and $V_Y = +110$ km s^{-1}. These two peaks correspond to the two components that appear to separate and merge in the observed profiles (Fig. 1). The MSO tomogram shows similar properties, with a strong peak near $V_X = -85$ km s^{-1} and $V_Y = -19$ km s^{-1} and an asymmetric extension into the upper right quadrant that corresponds to the weaker peak seen in the ESO tomogram. The differences are partially attributable to the lower resolution of the MSO spectra, but they may also reflect real differences in the emission between these epochs. In the next section, we explore how these tomograms can be interpreted in terms of gas flows into a colliding winds bow shock.

4. A Colliding Winds Model for HD 149404

Both stars in this system are expected to have significant stellar wind outflows based on their spectral classifications, and the presence of winds is evident in the strong UV P Cygni lines (Hutchings & Van Heteren 1981) and radio emission (Lamers & Leitherer 1993). Here we explore a wind outflow geometry that could potentially explain the orbital variations in the Hα emission. We present in Figure 6 a schematic drawing of HD 149404 as viewed from above the orbital plane, with dimensions from Penny et al. (1999). This view is probably very close to the way the binary actually appears in the sky, due to the low inclination ($i = 30°$) of the system. Based on the observed ellipsoidal variation, Penny et al. find that Star 1 is close to filling its critical Roche surface, and the diagram uses their estimates of volume equivalent radii, $R_1/R_\odot = 23$, $R_2/R_\odot = 16$, semimajor axis, $a/R_\odot = 62$, and mass ratio, $M_2/M_1 = 1.17$. The center of mass (*solid dot*) would be shifted toward Star 2 (from the illustrated position at $x/a = 0.54$ to 0.60) if the mass ratio from Stickland & Koch (1996) is adopted. The luminosities of the stars are almost identical according to Penny et al. (since Star 2 is hotter and smaller), and both should have comparable mass loss rates due to their radiatively driven winds. Penny et al. note that both stars are rotating faster than synchronously ($\Omega/\Omega_{\rm syn} = 1.4$ and 1.3 for Stars 1 and 2, respectively).

The tomograms provide several hints about the site of the Hα emission. The emission velocity distributions illustrated in Figures 4 and 5 are both centered on the system center of mass and show little or no evidence of orbital motion (which would displace the emission distribution along the V_Y-axis where the stars' orbital velocity components are situated). This central distribution implies that the emitting gas cloud is also centered on the system center of mass which is found in the gap between the stars (Fig. 6). A second clue about the placement of the emission comes from inspection of the differences between the observed and reconstructed profiles in Figures 1 and 2. We see that the tomographic reconstructions are generally a good match *except* at the conjunction phases (0.25 and 0.75). At both conjunctions, we find that the red, receding peak is stronger than expected while the blue, approaching peak is weaker. These properties suggest to us that we are witnessing emission that arises in gas streams along the axis between the stars. The fact that the receding gas is always preferred over the simple model results indicates that it originates in the closer outgoing stream, while the opposite approaching stream suffers some obscuration and must arise from the vicinity of the more distant star. Thus, we suggest that the bulk of the emission originates in gas flows from both stars that are moving toward a colliding winds shock zone between the stars.

This simple model explains the V_X components of motion, and the smaller V_Y components probably reflect the rapid rotation of the stars. Since both stars have

super-synchronous rotation rates, we expect that gas flows leaving their surfaces would share this motion. The smaller vectors placed between the stars in Figure 6 represent the vector sum of radial outflow and rotational deflection.

The model we envision is sketched in Figure 6. The winds of these luminous stars collide in the gap between the stars (shown as the shaded area). Note that the shock region illustrated is schematic only, whereas the actual shock boundary is defined by the balance of wind momenta. The winds of the stars themselves maybe concentrated towards the equatorial plane due to rapid rotation (Ignace, Cassinelli, & Bjorkman 1996) and/or focused toward the inner Lagrangian point by tidal effects (Friend & Castor 1982). The Hα emission appears to be strongest in the material flowing into the shock region, and in fact, the emission strength probably drops significantly in the shock itself because the Hα emissivity decreases with the higher temperatures found there (see Fig. 2 in Richards & Ratliff 1998). Once the gas cools as it moves out from the collision apex, it will once again emit more efficiently, and the broad distribution of emission flux in the tomograms probably reflects a large emission volume.

We can make an approximate estimate of the emission volume by calculating the total emission measure in Hα. We used the stellar dimensions adopted above and stellar fluxes from Kurucz (1994) together with the average observed equivalent width of $W_\lambda = -5.3$ Å to derive a total Hα emission measure of 2.6×10^{34} erg s^{-1}. Then, using an emissivity coefficient for an assumed temperature of 36000 K (Richards & Ratliff 1998) and a density of 10^{12} cm^{-3} (appropriate to the upper atmospheres of hot stars), we find an emitting volume of 2×10^{35} cm^3, equivalent to a sphere of radius $5R_\odot$. The gap between the stars is $\approx 18R_\odot$ along the axis, and so the observed emission measure is consistent with an origin roughly between the stars if our temperature and density estimates are reasonable.

In summary, the tomograms of the Hα emission profiles in HD 149404 suggest the presence of gas flows or focused winds that probably interact in a shock region. We find no evidence for present day mass transfer in the system, which suggests that the evolution of the binary is being driven by stellar wind mass loss from the entire system. Future observations of HD 149404 (particularly high resolution maps of the circumstellar gas surrounding the system) will help elucidate the nature of the colliding winds and the role this phenomenon plays in massive binary evolution.

We are deeply indebted to the Directors and Staff of MSO and ESO for their support of our observing runs. This research made use of the Simbad database, operated at CDS, Strasbourg, France. Institutional support was provided from the GSU College of Arts and Sciences and from the Research Program Enhancement fund of the Board of Regents of the

University System of Georgia administered through the GSU office of the Vice President for Research and Sponsored Programs. This work was partially supported by NASA ADP grant NAG 5-2979 and the California Institute of Technology. We gratefully acknowledge all this support.

REFERENCES

Bagnuolo, W. G., Jr., Gies, D. R., & Wiggs, M. S. 1992, ApJ, 385, 708

Conti, P. S., Leep, E. M., & Lorre, J. J. 1977, ApJ, 214, 759

ESA (European Space Agency) 1997, The Hipparcos and Tycho Catalogues, ESA SP-1200 (ESA/ESTEC, Noordwijk)

Friend, D. B., & Castor, J. I. 1982, ApJ, 261, 293

Gies, D. R., Bagnuolo, W. G. Jr., & Penny, L. R. 1997, ApJ, 479, 408

Gies, D. R., & Wiggs, M. S. 1991, ApJ, 375, 312

Gies, D. R., Wiggs, M. S., & Bagnuolo, W. G., Jr. 1993, ApJ, 403, 752

Hutchings, J. B. 1976, Publ. Dom. Ap. Obs. Victoria, 14, 355

Hutchings, J. B., & Van Heteren, J. 1981, PASP, 93, 626

Ignace, R., Cassinelli, J. P., & Bjorkman, J. E. 1996, ApJ, 459, 671

Jaschek, M., & Jaschek, C. 1974, A&A, 36, 401

Jaschek, M., Jaschek, C., & Kucewicz, B. 1964, ZfAp, 59, 108

Kaitchuck, R. H., Schlegel, E. M., Honeycutt, R. K., Horne, K. Marsh, T. R., White, J. C., II, & Mansperger, C. S. 1994, ApJS, 93, 519

Kaper, L., Fullerton, A., Baade, D., de Jong, J., Henrichs, H., & Zaal, P. 1998, in Cyclical Variability in Stellar Winds (ESO Astrophysics Symposia Series), ed. L. Kaper & A. W. Fullerton (Berlin: Springer-Verlag), 103

Kucewicz, B. 1963, PASP, 75, 192

Kurucz, R. L. 1994, Solar Abundance Model Atmospheres for 0, 1, 2, 4, 8 km/s, Kurucz CD-ROM No. 19 (Cambridge, MA: Smithsonian Astrophysical Obs.)

Lamers, H. J. G. L. M., & Leitherer, C. 1993, ApJ, 412, 771

Maeder, A. 1999, A&A, 347, 185

Mason, B. D., Gies, D. R., Hartkopf, W. I., Bagnuolo, W. G., Jr., ten Brummelaar, T., & McAlister, H. A. 1998, AJ, 115, 821

Massey, P., & Conti, P. 1979, in Mass Loss and Evolution of O-Type Stars, ed. P. Conti & C. de Loore (Dordrecht: Reidel), 501

Penny, L. R. 1996, Ph.D. dissertation, Georgia State University

Penny, L. R., Gies, D. R., & Bagnuolo, W. G., Jr. 1999, in Wolf-Rayet Phenomena in Massive Stars and Starburst Galaxies, Proc. IAU Symp. 193, ed. K. A. van der Hucht, G. Koenigsberger, & P. R. J. Eenens (San Francisco: ASP), 86

Puls, J. et al. 1996, A&A, 305, 171

Richards, M. T., Jones, R. D., & Swain, M. A. 1996, ApJ, 459, 249

Richards, M. T., & Ratliff, M. A. 1998, ApJ, 493, 326

Schaller, G., Schaerer, D., Meynet, G., & Maeder, A. 1992, A&AS, 96, 269

Stickland, D. J., & Koch, R. H. 1996, Observatory, 116, 145

Thaller, M. L. 1997, ApJ, 487, 380

Vanbeveren, D., & de Loore, C. 1980, A&A, 86, 21

Vreux, J. M. 1985, A&A, 143, 209

Wiggs, M. S., & Gies, D. R. 1992, ApJ, 396, 238

Wiggs, M. S., & Gies, D. R. 1993, ApJ, 407, 252

Fig. 1.— Hα line profiles obtained at ESO in 1995 plotted against heliocentric radial velocity and arranged in order of orbital phase (phase 0 corresponds to Star 1 maximum radial velocity). Solid lines represent the observations while dotted lines show model profiles reconstructed from the tomogram.

Fig. 2.— Hα line profiles obtained at MSO in 1996 (*thin lines*) and in 1997 (*thick lines*) plotted against heliocentric radial velocity and arranged in order of orbital phase. Solid lines represent the observations while dotted lines show model profiles reconstructed from the tomogram.

Fig. 3.— Hα equivalent width measurements as a function of orbital phase. Filled circles represent ESO observations, while open squares and circles represent MSO observations from 1996 and 1997, respectively.

Fig. 4.— A tomogram representation of the Hα emission from ESO observations. The grayscale image gives the emission intensity (as a fraction of the peak value) for the velocity structure seen in projection at different orbital phases. V_X refers to motion along the axis joining the stars while V_Y is perpendicular to this axis. Observations at orbital phases 0.0, 0.25, 0.5, and 0.75 correspond to projections of this image as seen from the left hand side, above, right hand side, and below, respectively. The open circles in white represent the $V \sin i$ limits of Star 1 (*below*) and Star 2 (*above*).

Fig. 5.— A tomogram representation of the Hα emission from MSO observations in the same format as Fig. 4.

Fig. 6.— A view of HD 149404 as seen from above the orbital plane. The dotted line indicates the classical Roche surfaces. The solid dark curves outline the presumed photospheres of the stars. Curved arrows inside the stars represent their equatorial rotation velocities. The center of mass is indicated by a solid dot on the axis joining the two stars, and orbital phases are shown on the periphery in the direction of the observer. The shaded area indicates the likely location of the colliding winds shock. The arrows between the stars show the vectors of the Hα emission peaks (thick line for the strong component and thin line for the weak) for the proposed gas flow configuration.

Table 1. Observations of HD 149404

HJD	Orbital Phase	W_λ (Å)	Observatory / Year
2449867.5899	0.0685	−4.89	ESO 1995
2449867.8031	0.0901	−4.87	ESO 1995
2449868.5400	0.1653	−4.51	ESO 1995
2449868.6741	0.1790	−4.77	ESO 1995
2449868.8327	0.1951	−4.59	ESO 1995
2449869.5451	0.2677	−4.81	ESO 1995
2449869.6552	0.2789	−4.88	ESO 1995
2449869.7825	0.2919	−4.71	ESO 1995
2449870.5891	0.3740	−4.28	ESO 1995
2449870.7447	0.3899	−4.22	ESO 1995
2449871.6361	0.4807	−4.41	ESO 1995
2449871.8134	0.4988	−4.29	ESO 1995
2449872.5903	0.5779	−4.35	ESO 1995
2449872.7294	0.5921	−4.42	ESO 1995
2449872.8544	0.6049	−4.48	ESO 1995
2449873.5600	0.6768	−4.58	ESO 1995
2449873.7567	0.6968	−4.53	ESO 1995
2449874.6598	0.7888	−4.65	ESO 1995
2449874.8359	0.8068	−4.51	ESO 1995
2450148.2334	0.6632	−5.53	MSO 1996
2450152.1624	0.0635	−6.54	MSO 1996
2450153.1770	0.1669	−7.25	MSO 1996
2450154.1908	0.2702	−7.02	MSO 1996
2450155.1266	0.3655	−6.00	MSO 1996
2450155.1385	0.3667	−6.45	MSO 1996
2450528.1580	0.3737	−5.53	MSO 1997
2450530.0721	0.5687	−6.55	MSO 1997
2450531.0629	0.6696	−7.22	MSO 1997
2450534.0516	0.9741	−7.02	MSO 1997
2450535.0399	0.1748	−5.99	MSO 1997
2450536.0366	0.1764	−6.46	MSO 1997
2450538.0418	0.3807	−6.50	MSO 1997

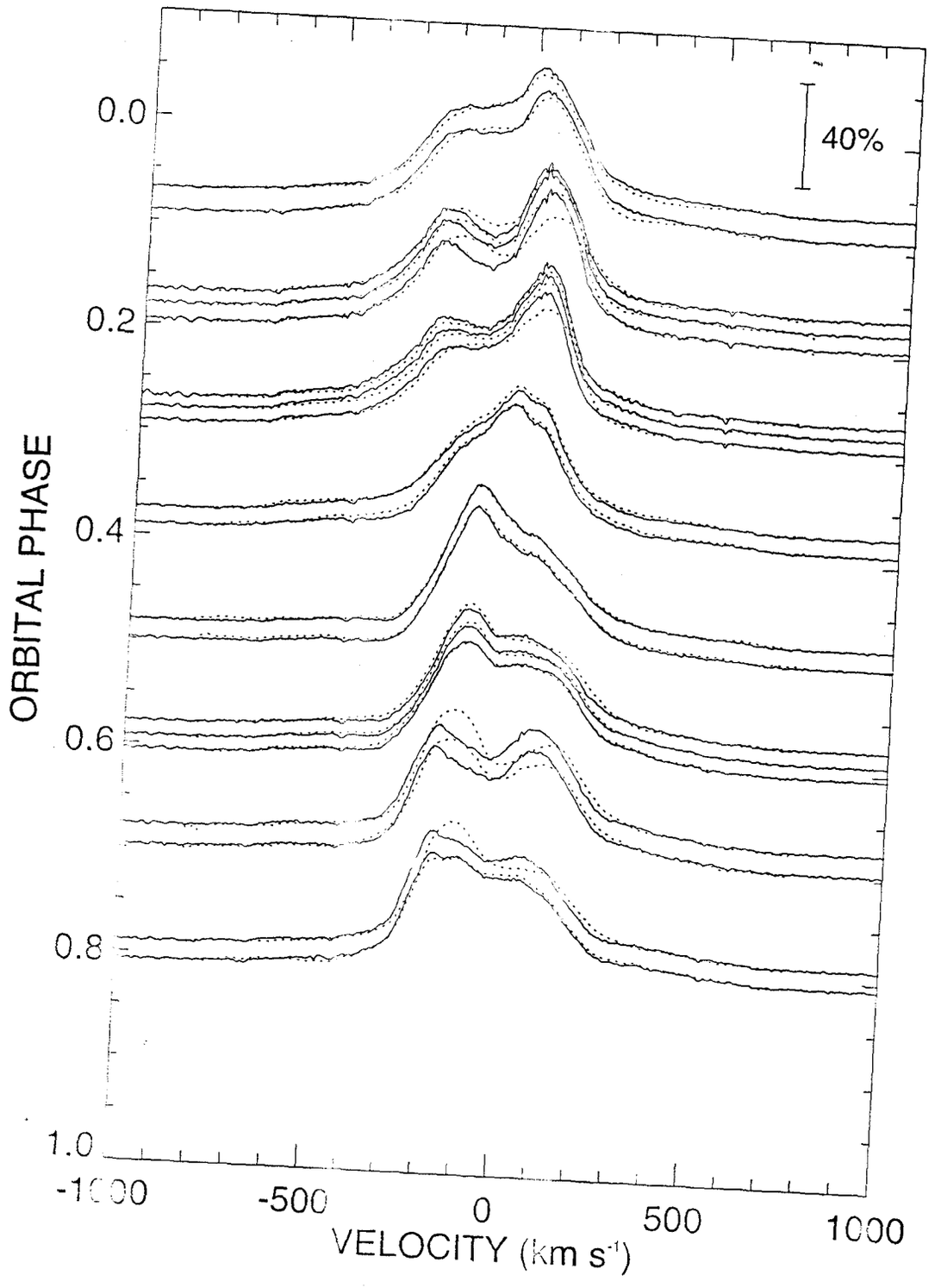
0.0
0.2
0.4
0.6
0.8
1.0
ORBITAL PHASE
40%
-1000
-500
0
500
1000
VELOCITY (km s-1)

Fig. 1.—

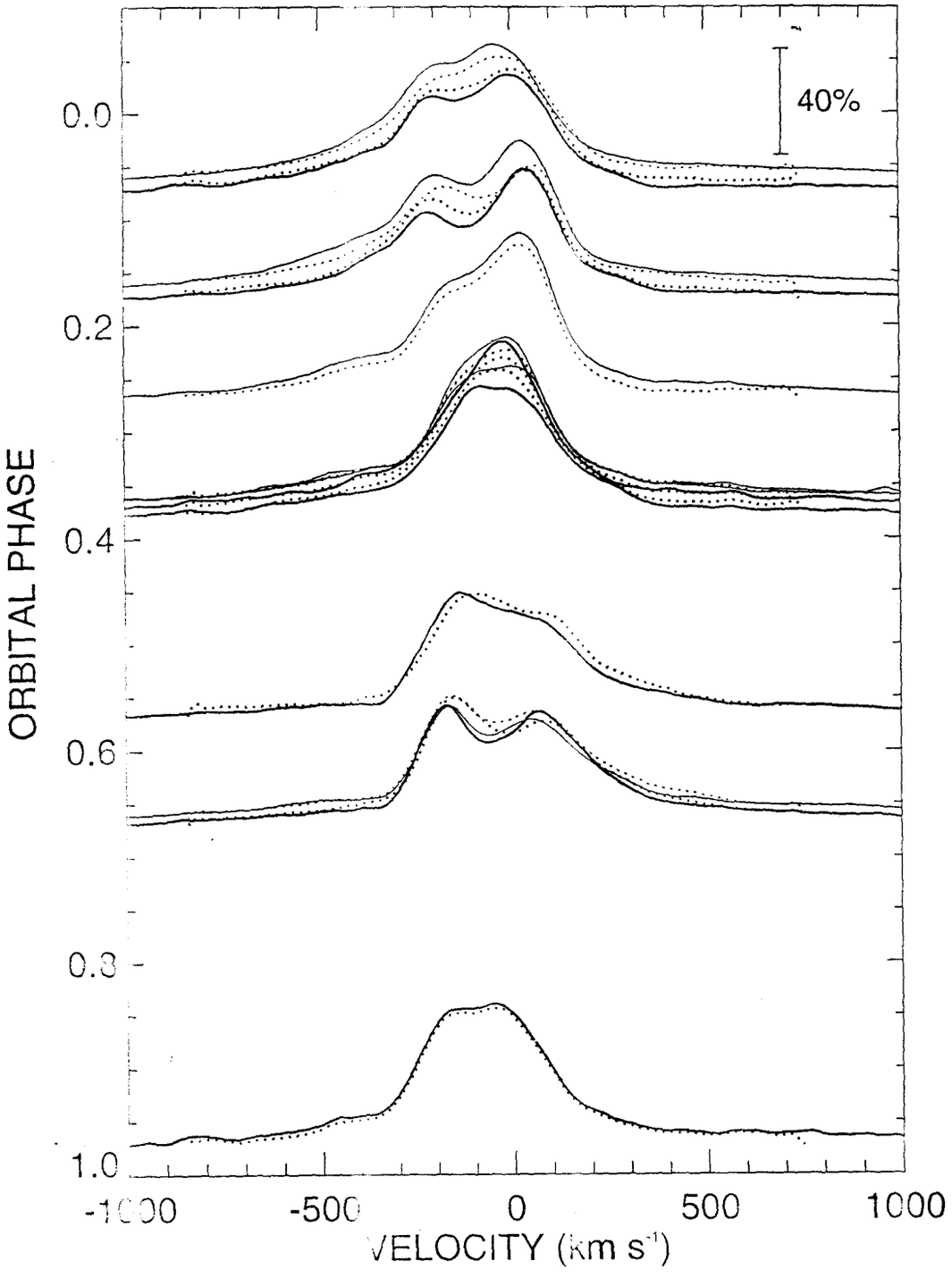
40%
0.0
0.2
0.4
0.6
0.8
1.0
ORBITAL PHASE
-1000
-500
0
500
1000
VELOCITY (km s^{-1})

Fig. 2.—

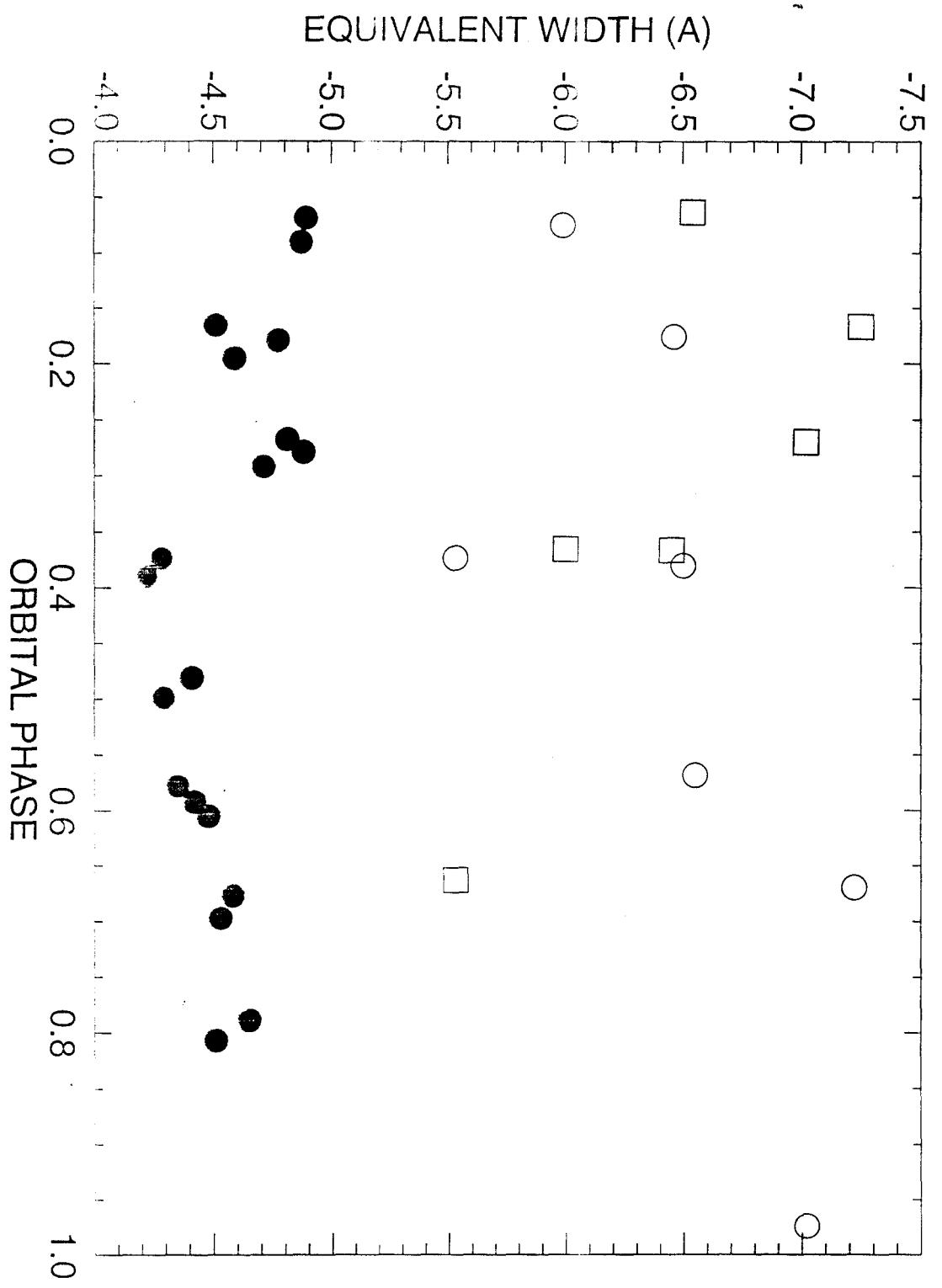
EQUIVALENT WIDTH (A)
-4.0
-4.5
-5.0
-5.5
-6.0
-6.5
-7.0
-7.5
ORBITAL PHASE
0.0
0.2
0.4
0.6
0.8
1.0

Fig. 3.—

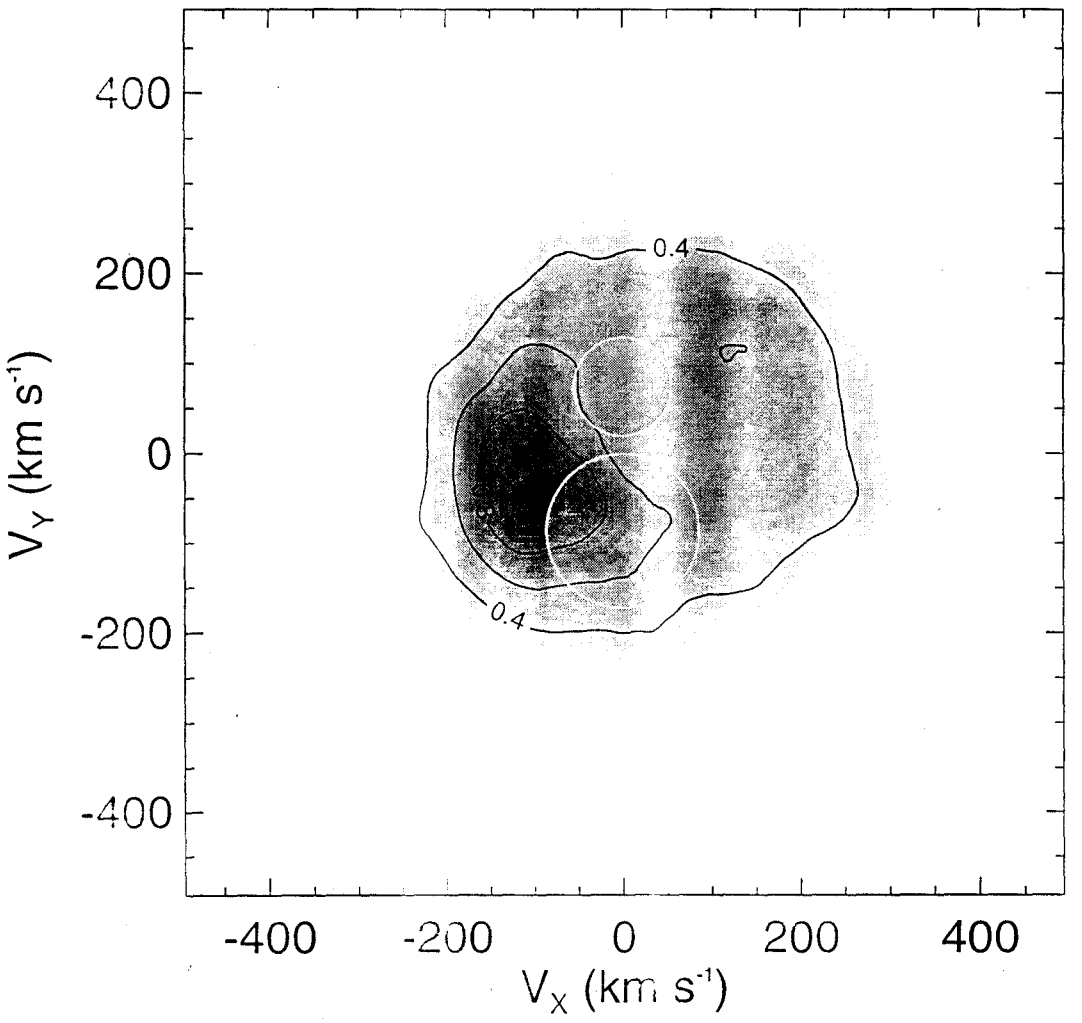

Fig. 4.—

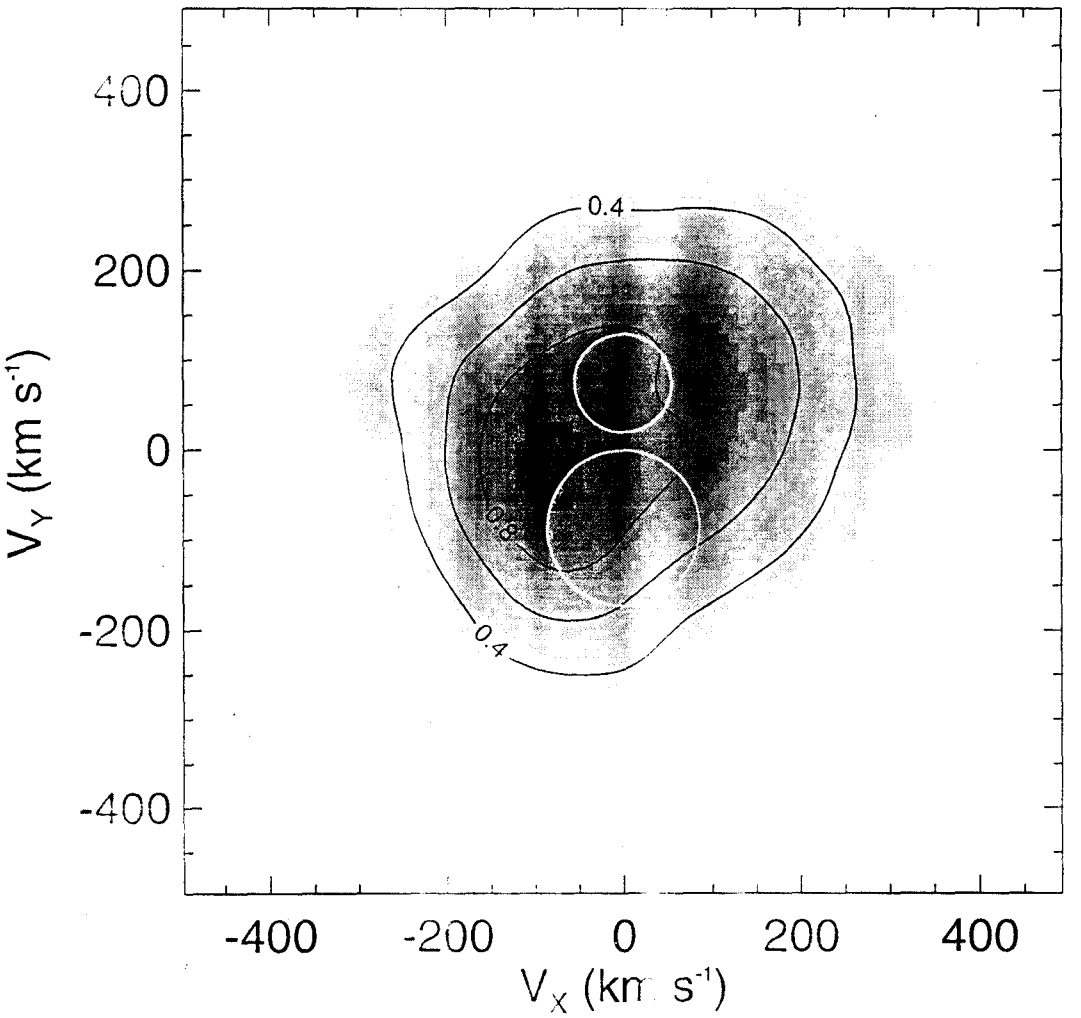

Fig. 5.—

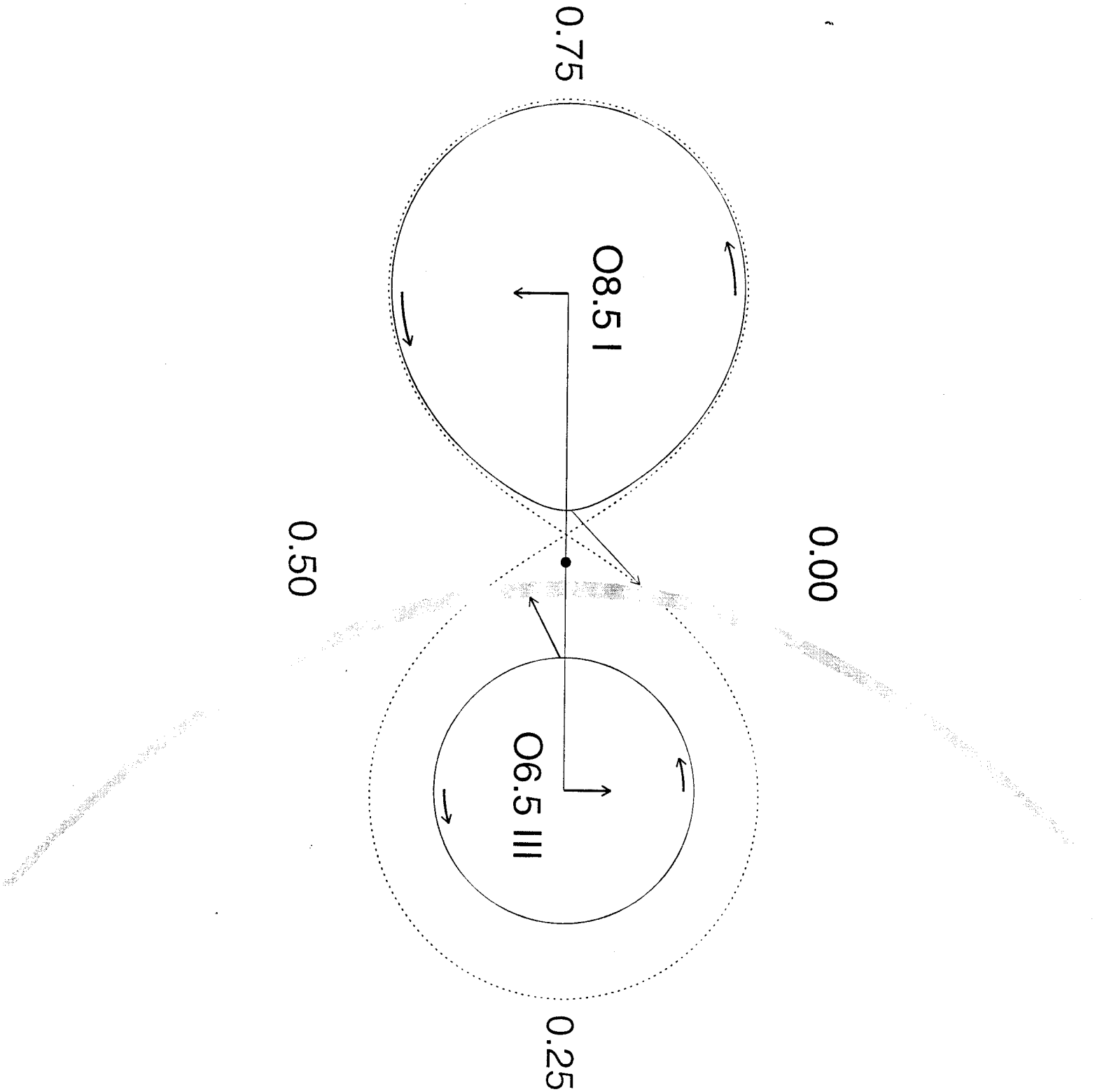

Fig. 6.—